Study of Self-Absorption of Emission Magnesium Lines in Laser-Induced Plasmas on Calcium Hydroxide Matrix

Diego M. Díaz Pace, Cristian A. D'Angelo, and Graciela Bertuccelli

***Abstract*—In this paper, we investigate the self-absorption of Mg I–II emission lines on laser-induced breakdown spectroscopy (LIBS) experiments. We produced the plasmas in air at atmospheric pressure by focusing a Nd:YAG laser onto a pellet of finely powdered calcium hydroxide with a concentration of 625 ppm of Mg and recorded the intensity profiles of Mg lines at different delay times after the laser pulse from plasmas generated with different laser energies. We carried out the analysis of the line profiles within the framework of a homogeneous plasma in local thermodynamic equilibrium by a computer algorithm that calculates the emission spectra and matches them to the experimental measurements. It allowed evaluation and compensation of self-absorption by using the spectroscopic information saved on the optical thicknesses of the lines. After that, we performed the characterization of the plasma and correlated the self-absorption features with the different trends of the temperature, the electron density, and the Nl parameters obtained. At the early times of plasma evolution, we found that the fast expansion of the plume was dominant and the self-absorption effects are difficult to interpret within the current approach, supplying only qualitative information. On the other hand, at later times, the results obtained could be properly analyzed showing the practical usefulness of the method to provide valuable information for both basic and applied LIBS research.**

***Index Terms*—Laser-induced breakdown spectroscopy (LIBS), plasma characterization, self-absorption.**

I. Introduction

LASER-INDUCED breakdown spectroscopy (LIBS) is a promising technique based on the spectral analysis of the radiation emitted by a laser-induced plasma (LIP) for determination of the elemental composition of liquids, gases, and solids. LIBS has attractive advantages such as the capability of rapid, *in situ*, and multielement measurement with a minimum of sample preparation. Recently, it has experienced a growing interest due to both emerging needs to carry out measurements under conditions not feasible with other well-established techniques and actual technology development in instrumentation (lasers, spectrographs, and detectors). Nowadays, the challenge is to improve the analytical performance of LIBS in a wide range of applications to integrate it to conventional analytical techniques [1].

Generally, obtaining qualitative results with LIBS does not present major problems. Nevertheless, carrying out a reliable semiquantitative or a quantitative analysis is not straightforward because the plasma spectral emission is determined not only by the concentration of the analyte in the sample but also by the properties of the plasma itself, which, in turn, depend on several factors such as the characteristics of the excitation source, the sample, and the surrounding atmosphere [2]. This fact makes LIPs very complex sources of radiation where the main difficulties that originated on applications in air at atmospheric pressure come from time evolution, spatial inhomogeneity, self-absorption, and matrix effects. In particular, the problem of determining the degree of self-absorption of spectral lines has been widely discussed in the literature [3]–[11]. Evaluation and correction of self-absorption is essential to LIBS measurements devoted to both basic and applied investigations since it constitutes one of the largest obstacles toward an accurate quantitative analysis as well as one of the main sources of systematic errors in LIPs diagnostics. It causes a reduction of the observed line intensities and additional broadening of the lines.

From an experimental point of view, the most common approach is the construction of calibration curves selecting those lines not suffering from strong self-absorption at the conditions of measurement [12]. However, the optically thin spectral lines are usually weak and seldom detected. In addition, reference samples may be unavailable in many practical situations, making impossible to construct a calibration curve (e.g., unique, complex, expensive, or unknown-matrix samples). An even more difficult task to be accomplished is to compensate the self-absorption suffered by the measured spectral lines to carry out an accurate plasma characterization. A recent review by Tognoni *et al.* [13] summarizes the current state of the art on this topic related to applications of the CF-LIBS method and emphasizes the necessity of further investigation. In this scenario, plasma characterization by determining the temperature, the electron density, and the atom/ion densities of the different species present in the plume taking into account self-absorption effects is of paramount importance to select suitable conditions of measurement in analytical applications and to provide a valuable feedback in plasma modeling.

The aim of this paper is to study the self-absorption of Mg I–II emission lines during the temporal evolution of

Manuscript received August 24, 2011; revised November 3, 2011; accepted December 19, 2011. Date of publication January 31, 2012; date of current version March 9, 2012. This work was supported in part by the Consejo Nacional de Investigaciones Científicas y Técnicas (CONICET) and in part by Comisión de Investigaciones Científicas de la Pcia. de Bs. As. (CICPBA).

The authors are with the Instituto de Física "Arroyo Seco", Facultad de Ciencias Exactas, Universidad Nacional del Centro de la Provincia de Buenos Aires, 7000 Tandil, Argentina (e-mail: ddiaz@exa.unicen.edu.ar; cdangelo@exa.unicen.edu.ar; gbertucc@exa.unicen.edu.ar).

Digital Object Identifier 10.1109/TPS.2011.2181875

plasmas generated with different laser pulse energies on samples with a calcium hydroxide matrix. The self-absorption features of the measured lines are correlated with the thermodynamic parameters obtained from plasma characterization to investigate some of the underlying physical processes in plasma dynamics.

II. Theoretical: Spectral Line Emission From a Homogeneous Plasma in LTE

We consider a cylinder-symmetrical homogeneous plasma in local thermodynamic equilibrium (LTE). The emission and absorption of radiation are described by an emission coefficient ε_λ (J s^{-1} m^{-3} sr^{-1} nm^{-1}) and an absorption coefficient $\kappa(\lambda)$ (m^{-1}), respectively. The spectral intensity I_λ (J s^{-1} m^{-2} sr^{-1} nm^{-1}) emitted along the line of sight is given by solution to the equation of radiation transfer [14]

$$I_\lambda = CU_\lambda(T)\left(1 - e^{-\tau_\lambda(T)}\right) \tag{1}$$

where C (a. u.) is a factor that unifies units and depends on the instrumental setup, U_λ (W m^{-2} sr^{-1} nm^{-1}) is the distribution for blackbody radiation, and τ_λ (dimensionless) is the optical thickness of the plasma, which can be can be expressed by [3]

$$\tau_\lambda(T) = \kappa(\lambda)l = \kappa_e(T)NlP(\lambda) \tag{2}$$

where $\kappa_e(T)$ (m^3) is a coefficient depending on the atomic parameters of the transition and the plasma temperature T (K), namely

$$\kappa_e(T) = \frac{\lambda^4}{8\pi c Q(T)} A_{ji} g_j e^{-E_i/kT}\left(1 - e^{E_i - E_j/kT}\right) \tag{3}$$

where λ_0 (m) is the central wavelength of the line, A_{ji} (s^{-1}) is the transition probability, g_j (dimensionless) is the degeneracy of the upper energy level, and E_i, E_j (eV) are the energy of the levels; N (m^{-3}) is the density of the emitting element in the plasma, l (m) is the length of the plasma along the line of sight, $P(\lambda)$ (m^{-1}) is the normalized line profile, in general described by a Voigt function, and $Q(T)$ (dimensionless) is the atomic partition function. The coefficient κ_e describes the influence of the spectroscopic parameters of spectral lines on the optical thickness; thus, it is useful to predict the relevance of self-absorption for a given transition [3].

The optical thickness τ_λ of a given transition reaches a maximum τ_0 at the line center λ_0. If self-absorption of radiation within the plasma is negligible, $\tau_0 \ll 1$, and the plasma is said to be optically thin. On the other hand, for the stronger lines, which are generally the resonance, the radiation emitted has a large probability of being absorbed, then $\tau_0 \gg 1$, and the plasma is said to be optically thick.

As mentioned by Moon *et al.* in [9], a correction factor R_λ (adim.), defined as

$$R_\lambda \equiv \frac{I_\lambda^{\text{thin}}}{I_\lambda^{\text{thick}}} = \frac{\tau_\lambda}{1 - e^{-\tau_\lambda}} \tag{4}$$

can be calculated based on the optical thickness and subsequently applied to the experimental profiles to retrieve the optically thin line profiles for the same number density of emitters. Namely

$$I_\lambda^{\text{thin}} = R_\lambda I_\lambda^{\text{thick}}. \tag{5}$$

In order to quantify the effect of self-absorption on the emission intensity of a given line, a SA coefficient can be defined using the ratio of the measured peak intensity over its value in the absence of self-absorption

$$SA \equiv 1 - \frac{I^{\text{thick}}(\lambda_0)}{I^{\text{thin}}(\lambda_0)} = 1 - \frac{1}{R_0} \tag{6}$$

where R_0 is the particular value of R_λ at the line peak (λ_0). Hence, $SA = 0$ if the line is optically thin and it increases up to 1 as the line becomes self-absorbed.

Integrating both sides of (2) along the line profile

$$A \equiv \int_{\text{line}} \tau_\lambda d\lambda = \kappa_e(T)Nl \tag{7}$$

we obtain

$$Nl = \frac{A}{\kappa_e(T)} \tag{8}$$

which is the product of the particle density (atoms/ions) (m^{-3}) and the optical length of the plasma (m) along the line of sight. As already mentioned by Aguilera and Aragón in [7] and [8], the parameter Nl is relevant to complete the description of the plasma emission provided by the plasma temperature and the electron density.

III. Experiment

A. Experimental Setup

The experimental setup is very similar to that used in a previous work [15]. It is a LIBS system with good spectral resolution, based on a monochromator equipped with a photomultiplier detector (PM), suitable for detailed line profile measurements (Fig. 1). The plasmas were generated in air at atmospheric pressure by focusing a Nd:YAG laser (Continuum Surelite II, $\lambda = 1064$ nm, 7-ns pulse FWHM, pulse energy up to 200 mJ, and repetition rate of 4 Hz), using a quartz lens of 100-mm focal length, at right angles onto a pressed pellet of finely powdered calcium hydroxide with a concentration of 625 ppm of Mg. In order to avoid the breakdown in air, the lens-to-sample distance was lower than the focal length of the lens in such a way that the waist of the focused beam was placed at a position d below the sample surface by using a micrometer translation stage. The pulse energy, which was measured with a calorimeter, was varied by employing an optical attenuator. The light emitted by the plasma was collected at right angles to the laser beam direction and imaged on the entrance slit (50-μm width) of a spectrograph (Czerny-Turner, resolution of 0.01 nm at $\lambda = 300$ nm, focal length of 1.5 m, and grating of 2400 lines/mm) using a second quartz lens. The spectral emission was detected with the PM spatially integrated along the line of sight. All measurements were time resolved and

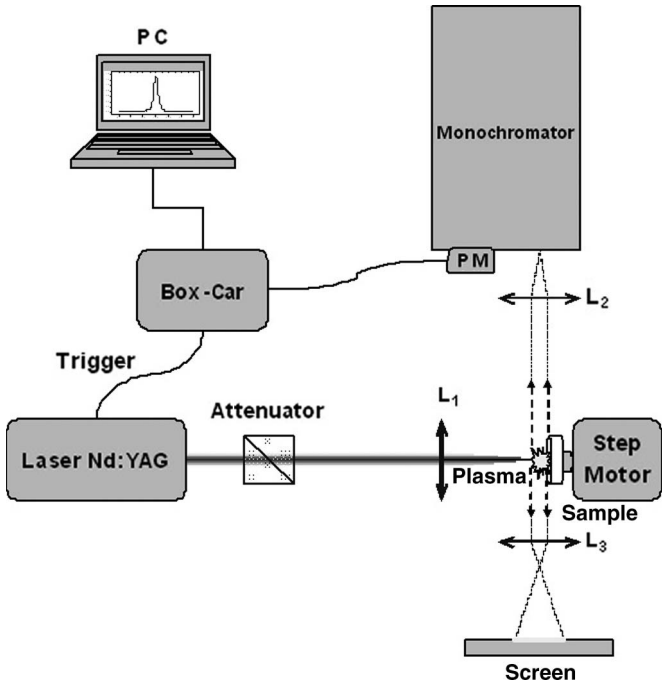

Fig. 1. Experimental setup used for LIBS measurements.

TABLE I
SPECTROSCOPIC PARAMETERS OF NEUTRAL (I) AND SINGLE IONIZED (II) ATOMIC LINES ANALYZED (DATA FROM NIST DATABASE)

Element	λ (nm)	A_{ji} (10^8 s^{-1})	E_i (eV)	E_j (eV)	g_i	g_j
Mg I	278.14	5.43	2.711	7.168	3	1
Mg I	278.30	2.14	2.717	7.170	5	3
Mg I	285.21	4.91	0.000	4.346	1	3
Mg II	279.08	4.01	4.422	8.864	2	4
Mg II	279.55	2.60	0.000	4.434	2	4
Mg II	279.80	4.79	4.434	8.864	4	6
Mg II	280.27	2.57	0.000	4.422	2	2

averaged with a Box-Car employing suitable delay and gate times with respect to the laser pulse. During the measurements, the sample rotates slowly to avoid the formation of a deep crater on the sample surface. The experimental spectral lines were recorded by scanning the monochromator and recording the signal with the PM, where each point of the emission profile was obtained averaging for ten laser shots to improve the signal-to-noise ratio (SNR). The shape of the plasma was visualized during the experiment employing a lens to form a magnified lateral image (1:5) of the plume on a screen. Finally, the spectra were processed by a PC. The calculated incident laser irradiance on the sample surface was in the range of 4.5–18 GW/cm^2. It was estimated from the laser energies and the areas of the craters originated by the laser pulses on the sample surface by using a microscope equipped with an image acquisition system (Reichert MeF2 Optical Microscope).

B. Measurements and Analysis

We selected for the analysis seven close lines of Mg I and Mg II which are isolated and free from interference of other elements or substrate, listed in Table I. We investigated self-absorption of the Mg lines by measuring their experimental profiles with different delay times and different laser energies. We obtained quantitative information by relating the experimental results to the basic physics of the LIP emission, assuming a homogeneous plasma in LTE. The second assumption is generally valid in LIBS experiments because of the sufficiently large electron densities achieved ($\sim 10^{17}$ cm^{-3}). A criterion proposed by McWhirter [12] for LTE to hold in a plasma is based on the existence of a critical electron density for which the collisions with electrons dominate over the radiative processes, namely, $N_e^0 = 1.6 \times 10^{12} T^{1/2} (\Delta E)^3$ cm^{-3}, where T (K) is the temperature and ΔE is the energy gap difference between the transition levels. On the contrary, the first assumption is difficult to be fulfilled in LIPs generated in air because significant gradients of temperature exist. For this reason, we maintained a fixed focusing position of approximately $d = 4$ mm during the experiment since we have found that, in our experimental conditions, for such an optimal value of d, the plasmas generated have a maximum spectral emission for Mg and a more spherical shape than in other conditions, as already described by Aguilera and Aragón [16]. In this way, the spatial inhomogeneity is minimized. Even though we obtained "near-homogeneous" plasmas with this laser focusing distance, the assumption of a uniform distribution of the thermodynamic parameters within the plume is considered only as an approximation. We carried out the analysis of the line profiles employing a computer algorithm that calculates the emission spectra in the current approach and matches them to the experimental measurements [17]. It is based on obtaining the wavelength-dependent optical thicknesses (τ_λ) from which the features of the different spectral lines are derived, as explained in the following.

To calculate the line profiles, we considered that, in typical LIBS experimental conditions, the Stark effect and the instrumental function are, respectively, the dominant broadening mechanisms that determine the Lorentzian and Gaussian components of the Voigt profiles of the lines [18]. We took the necessary broadening parameters at a given plasma temperature from Griem's database [19]. For the 50-μm-width entrance/exit slits of the monochromator, the estimated instrumental width was 0.0065 nm. Then, using the spectroscopic data of the Mg lines available at the NIST Database [20] and varying two independent parameters, namely, the maximum optical thickness at the line center (τ_0) and the Stark width (w_{Stark}) within an estimated range of values (typically, $\tau_0 = 0.1$–10 and $w_{\mathrm{Stark}} = 0.01$–0.20 nm in our experiment), a fitting least squares iterative procedure calculated the optical thickness of each line by convolution of the Lorentzian and Gauss functions. Hence, we determined the theoretical profiles that best reproduced the experimental lines. Next, we evaluated the SA coefficients and performed the correction for self-absorption by applying the correction factor (4) to the intensity line profiles. In this way, a more accurate determination of the plasma parameters can be achieved. In fact, once we analyzed all experimental lines, we determined the electron density and the temperature with the optically thin line intensities from the Stark broadening and the Saha–Boltzmann plot methods, respectively. Moreover, we obtained the parameters Nl (m^{-2})

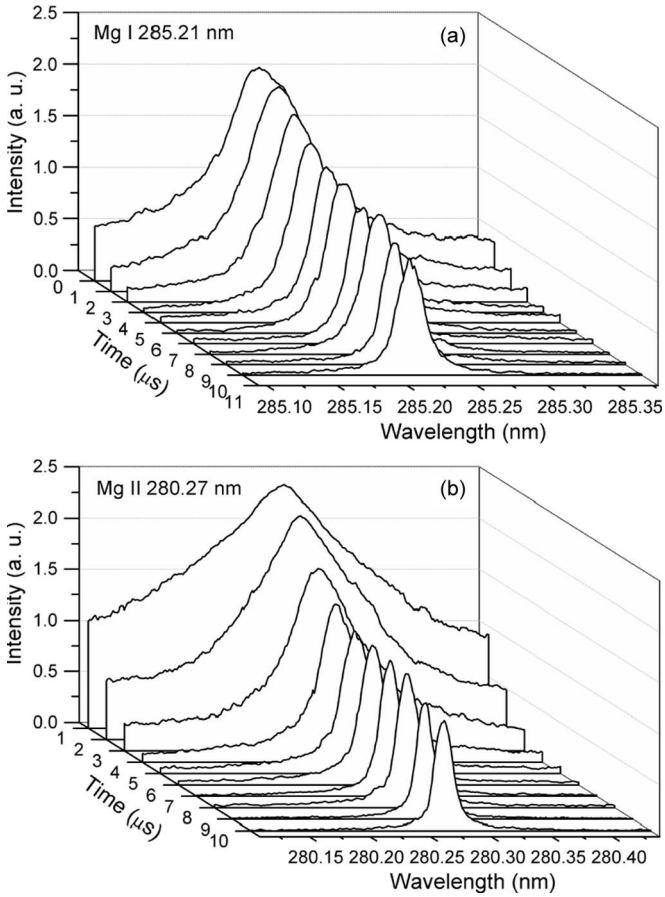

Fig. 2. Experimental intensity profiles of the lines (a) Mg I 285.21 nm and (b) Mg II 280.27 nm measured at several delay times. Laser energy: 100 mJ.

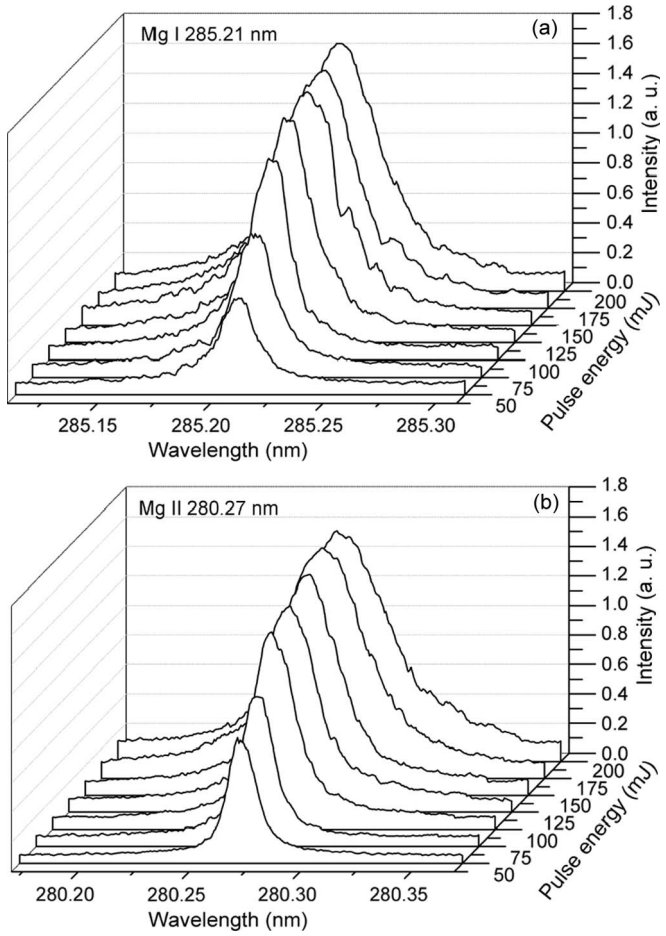

Fig. 3. Experimental intensity profiles of the lines (a) Mg I 285.21 nm and (b) Mg II 280.27 nm measured from plasmas generated with different laser energies. Delay: 7 μs, gate: 1 μs.

using (7) and (8) together with the plasma temperature and the factors $\kappa_e(T)$ previously calculated from (3). We executed systematically the procedure for all the Mg lines of Table I measured in different experimental conditions. Nevertheless, in some cases, the weak nonresonance Mg lines were recorded with a very low SNR, so they were not considered for the fitting procedure due to the high uncertainty associated to the calculated parameters.

IV. Results

A. Self-Absorption: Temporal Evolution and Laser Irradiance Effects

In order to obtain information about the physical LIP conditions, we investigated the temporal evolution of self-absorption as well as the effects of the laser energy on self-absorption. We measured the spectral lines of Mg at different times with a fixed pulse energy of $E = 100$ mJ. We varied the delay time with respect to the laser pulse in the range of 1–10 μs with a gate width of 1 μs. We also measured the lines with different laser energies, in the range of 50–200 mJ varying in steps of 25 mJ, with a fixed time window (delay: 7 μs, gate: 1 μs). As an example, Figs. 2 and 3 show the profiles of the lines Mg I 285.21 nm and Mg II 280.27 nm recorded at several delays from the laser pulse and from plasmas generated with different laser pulse energies, respectively.

In order to calculate the self-absorption coefficients of the Mg lines by using (6), we fitted the experimental profiles to obtain their optical thicknesses. The SA coefficients are shown in Fig. 4 as a function of the delay time. Different trends are observed for atomic and ionic lines. The Mg I line 285.21 nm becomes strongly self-absorbed for all the times analyzed where self-absorption grows slightly, reaching a maximum $(\text{SA} \sim 80\%)$, and then, it decreases smoothly at the last times of the interval. On the other hand, for Mg II resonance lines 279.55 and 280.27 nm, the trend of self-absorption shows an abrupt increase during the first 3 μs ($\text{SA} \sim 20\%-30\%$ to $\sim$60%), and after that, a plateau is reached ($\text{SA} \sim 70\%-90\%$). Particularly, the degree of self-absorption of the line 279.55 nm is larger than that of the line 280.27 nm. In addition, the nonresonance Mg lines show also different behaviors. While the trend of the Mg II lines 279.0 and 279.8 nm decreases monotonically after suffering a significant self-absorption during the first 3 μs ($\text{SA} \sim 70\%-80\%$), a more complex behavior appears for the Mg I lines 278.1 and 278.3 nm characterized by a moderate peak of absorption $(\text{SA} \sim 50\%)$ for intermediate delays of 3–4 μs.

We report in Fig. 5 the SA coefficients calculated for the Mg lines versus the laser irradiances. We see that the Mg I–II resonance lines are strongly self-absorbed for all the irradiances

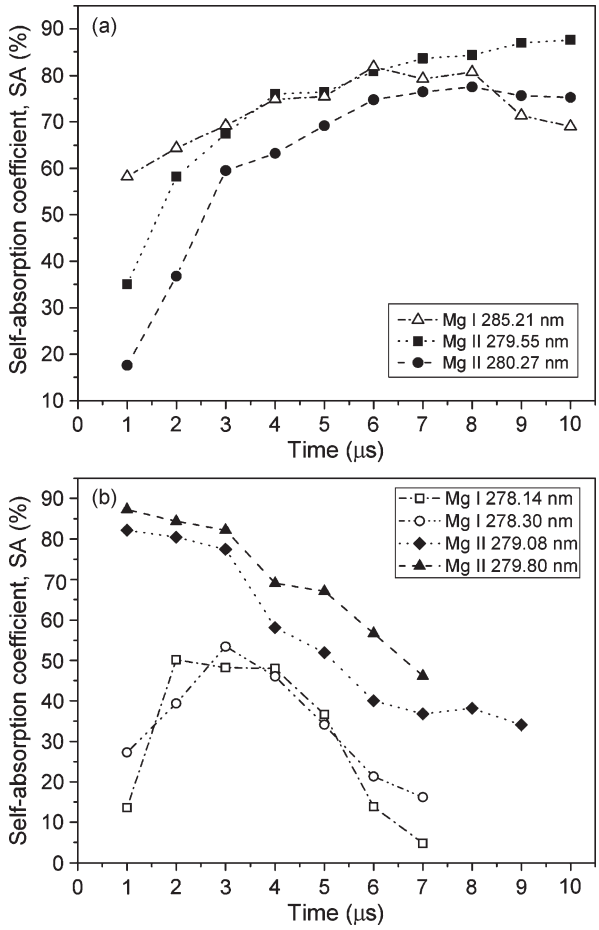

Fig. 4. Temporal evolution of self-absorption coefficients of (a) resonance and (b) nonresonance Mg I–II lines. Laser energy: 100 mJ.

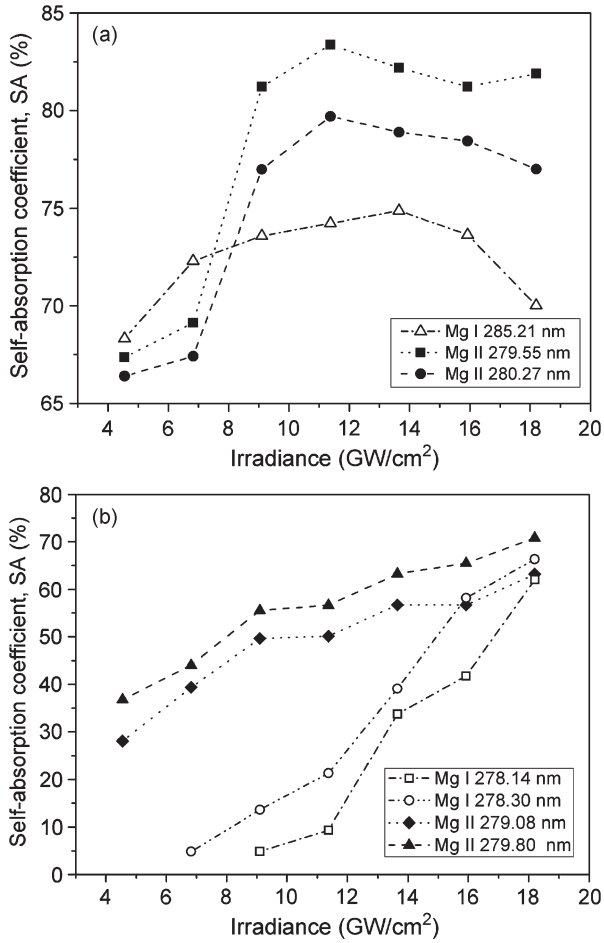

Fig. 5. Self-absorption coefficients of (a) resonance and (b) nonresonance Mg I–II lines for different laser irradiances. Delay: 7 μs, gate: 1 μs.

investigated (SA $\sim$ 70%–85%). We observed a slight increment at medium and high irradiances, where the Mg II line 279.55 nm is more absorbed than the Mg II line 280.27 nm. In addition, the Mg I line 285.21 nm is less affected by self-absorption than the Mg II lines for the same irradiances. In turn, the trend of nonresonance atomic and ionic lines of Mg shows an increment of self-absorption (SA $\sim 5\%-30\%$ to 70%), mainly appreciable for Mg I lines.

B. Line Parameters and Plasma Characterization

We interpreted the results exposed in the previous section based on the characterization of the plasmas. We calculated the emission intensities and Stark widths of Mg lines, as well as the temperature, the electron density, and the Nl parameters of the plasma from the fittings of the experimental spectra acquired. We calculated the plasma temperature using the Saha–Boltzmann plot method with the line intensities corrected for self-absorption. We derived the electron density from the observed Stark broadenings of the resonance Mg lines according to the approximated formula $w_{\mathrm{Stark}} = 2w\,(N_e/10^{16})$, where w_{Stark} is the experimental line width and w is the electron-impact (half) width parameter tabulated by Griem [18]. We obtained the Nl parameters for atoms and ions from the optical thicknesses of the corresponding resonance spectral lines.

Temporal Evolution: We reported in Fig. 6 the trend of the integrated line intensities as a function of the delay time. The emission of both Mg I and Mg II lines declines quickly during the first 5 μs. In addition, we observed the same behavior for the Stark widths, which show an exponential decrease with time (Fig. 7). The Mg II lines 279.55 and 280.27 nm, belonging to the same multiplet, have approximately equal Stark widths, which are larger than that of the Mg I line 285.21 nm mainly in the first 5 μs [Fig. 7(a)]. The resonance lines are broadened in a larger extent than the nonresonance lines and present a more pronounced relative variation. On the other hand, the Stark widths of the nonresonance lines of Mg I–II are smaller and exhibit a lower relative variation [Fig. 7(b)]. Thus, we employed only the resonance lines for the calculus of the electron density and the parameters Nl.

We show in Fig. 8 the calculated plasma temperatures, electron densities, and parameters Nl as a function of the delay time. The temperature and electron density of the plasma show exponential decays as time progresses. The figure also shows the calculated minimum electron number density values ($N_e^0 \sim 1 \times 10^{16}$ cm^{-3}) necessary to satisfy LTE conditions according to the McWhirter criterion. Even though the criterion is satisfied for all the times analyzed suggesting that LTE may exist, it is not sufficient to assure LTE conditions. The plot of the parameters Nl for Mg I and Mg II shows a step decreasing

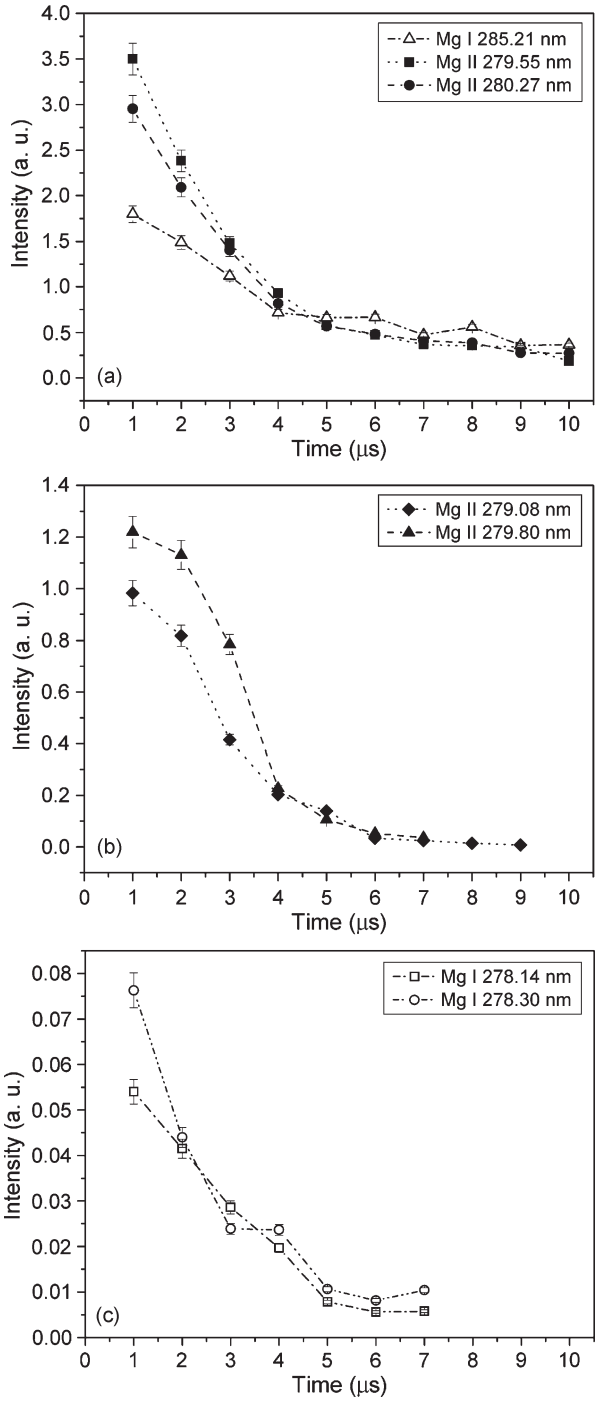

Fig. 6. Temporal evolution of the total intensities of Mg I–II lines. Laser energy: 100 mJ. The relative errors are on the order of 5%.

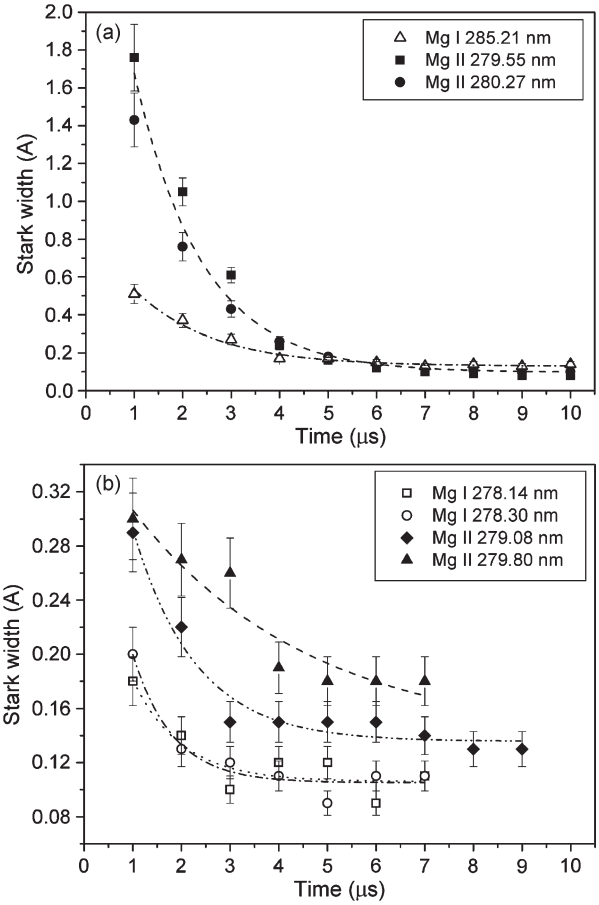

Fig. 7. Temporal evolution of Stark widths of (a) resonance and (b) nonresonance Mg I–II lines. Laser energy: 100 mJ. The estimated relative errors are on the order of 10%.

trend during the first 4 μs, where $Nl_{\mathrm{Mg\ I}}$ is significantly larger than $Nl_{\mathrm{Mg\ II}}$. At the later times of the interval analyzed, they are of the same order and remain approximately constant.

Effects of the Laser Irradiance: In Fig. 9, it is shown that the line intensities of Mg I–II lines increase monotonically with the laser irradiance. The trend of the Stark widths is shown in Fig. 10. We observed that the broadenings of the resonance lines rise exponentially with the irradiance. In turn, the nonresonance lines have smaller broadenings which result to approximately constant values for the range of irradiances studied. Consequently, we used the Stark widths of the resonance lines for the calculus of the electron density. The broadening of the Mg I line 285.21 nm is larger than that of the Mg II lines 279.55 and 280.27 nm, which have approximately the same Stark width since they belong to the same multiplet, except for the higher energies where the broadenings of the three resonance lines are comparable.

The calculated values of the plasma temperature, electron density, and Nl parameters are shown in Fig. 11, where an increasing trend is observed with respect to the laser irradiance. In the case of the temperature, we observe a linear growth, while the electron density exhibits a modest exponential increment. The calculated minimum electron number density values ($N_e^0 \sim 1 \times 10^{16}$ cm^{-3}) necessary to satisfy LTE conditions according to the McWhirter criterion are shown. As in the previous case, the criterion is satisfied for all the range of irradiances, suggesting that LTE may exist. In addition, a strong increment of the Nl parameters occurs with the irradiance, showing that $Nl_{\mathrm{Mg\ II}}$ is larger than $Nl_{\mathrm{Mg\ I}}$.

V. Discussion

In order to gain a better insight into some of the physical processes occurring in the LIP, we correlated the self-absorption effects with the different trends of the thermodynamic parameters of the plasma (i.e., temperature, electron density, and Nl parameters) with the acquisition delay time

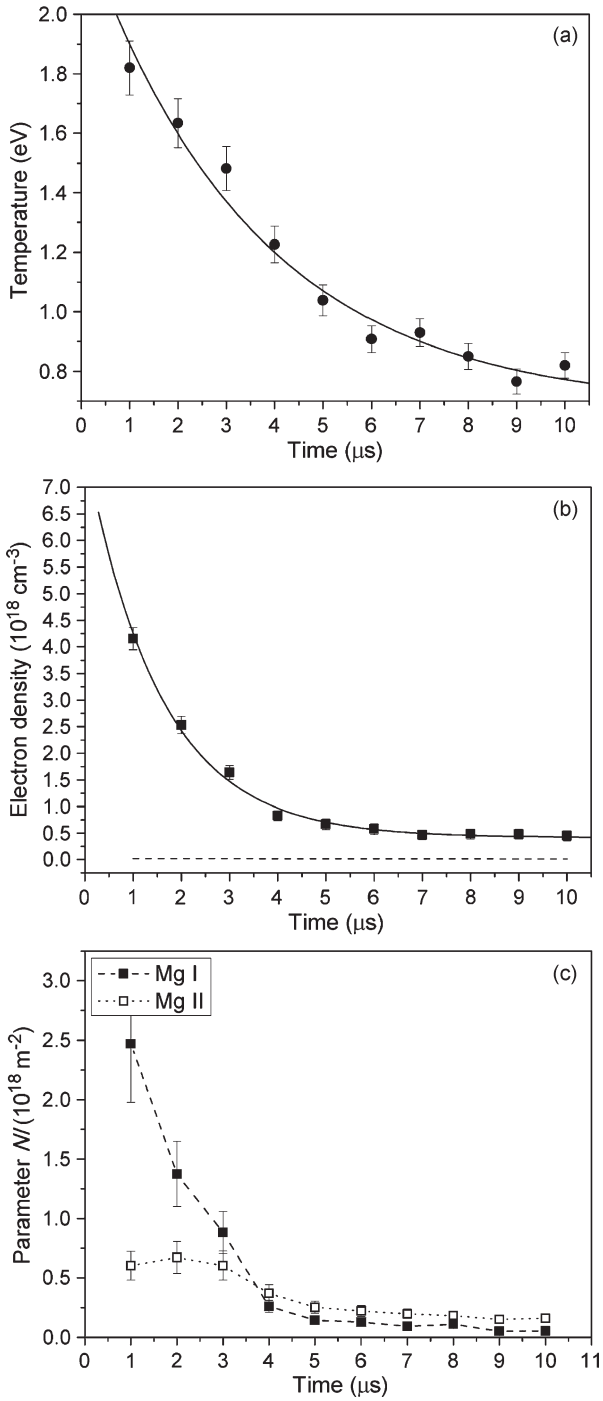

Fig. 8. Temporal evolution of (a) temperature, (b) electron density, and (c) Nl parameters of Mg I–II lines. Laser energy: 100 mJ. The dashed line indicates the minimum electron number density for the plasma to be in LTE at different delay times. The error in the calculus of the electron density was of 5%–10%, estimated from the propagation of the errors in the measurement of the Stark width and from Stark parameters. The estimated relative errors in Nl parameters are on the order of 20%.

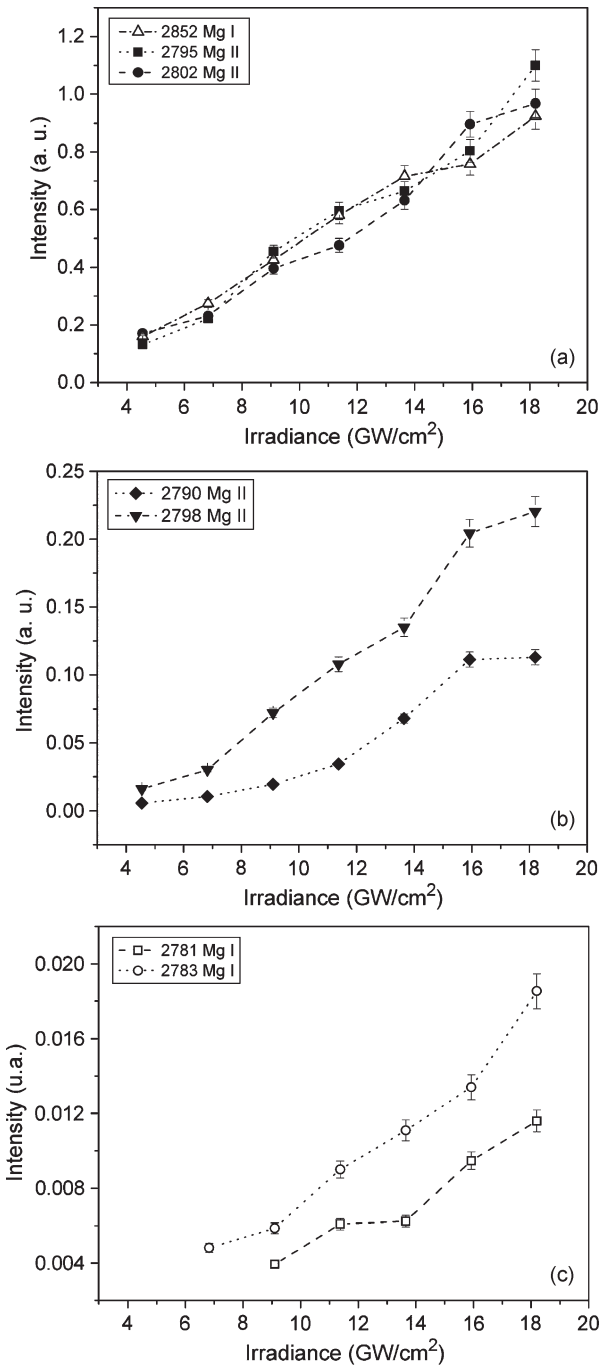

Fig. 9. Total line intensities of Mg I–II lines for different laser irradiances. Delay: 7 μs, gate: 1 μs. The relative errors are on the order of 5%.

after the laser pulse and with the laser irradiance employed to generate the plasmas. Before starting the discussion, it is worth stressing that the results have been calculated from the spectra obtained via integration of the measured emission intensity along the line of sight under the assumption of plasma homogeneity. Since this method is adopted in the majority of practical LIBS experiments described in the literature, the analysis drawn is believed to be analytically useful. The real, and also more complex, plasma features may be further investigated using more realistic plasma models, such as those reported in [21] and the references therein.

From (2), it can be deduced that the optical thickness of spectral lines, which governs self-absorption [see (4) and (6)], is determined by the product $\kappa_e(T)N$, which gives the population density of the lower energy level of the transition, the plasma length l along the line of sight, and the normalized line profile $P(\lambda)$. The optical thickness reaches its maximum value τ_0 at the line center and decreases toward the line wings. Thus, considering the simple assumption that the line is

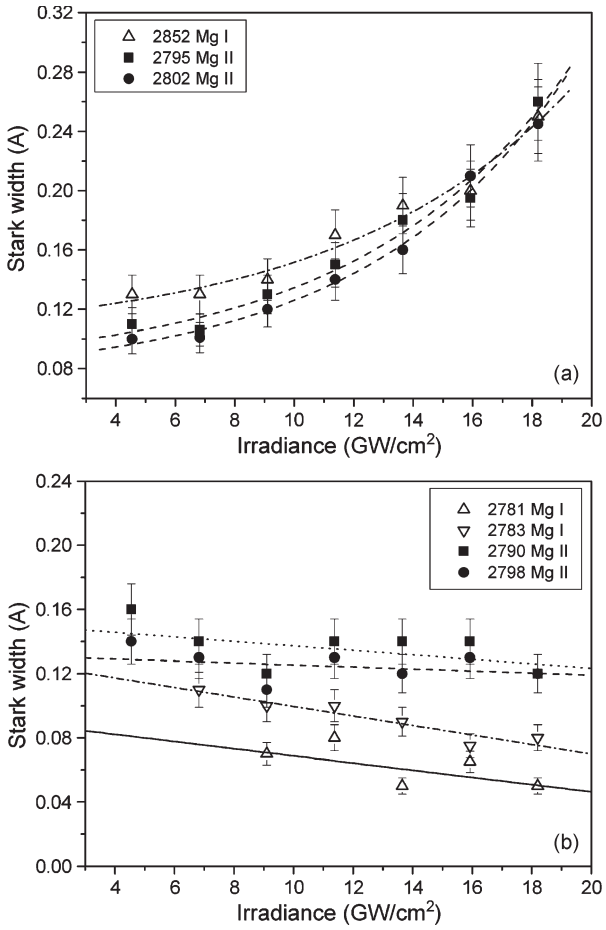

Fig. 10. Stark widths of (a) resonance and (b) nonresonance Mg I–II lines for different laser irradiances. Delay: 7 μs, gate: 1 μs. The estimated relative errors are on the order of 10%.

broadened only by the Stark effect and it has a Lorentzian profile, we have

$$\tau_0 \propto \frac{\kappa_e(T) N l}{N_e}. \tag{9}$$

From this expression, we see that the variation of self-absorption depends on the temperature, the density of species (atoms, ions, and electrons), and the size of the emitting plasma. In addition, several mechanisms take place simultaneously during the dynamic behavior of the plasma, as listed in the following.

1) As a consequence of changes of plasma temperature, the equilibrium between atoms and ions determined by the electronic density is modified according to the Saha equation [22]. A rise of temperature originates a higher ionization of the plasma. Such a growth of the electron density causes a larger broadening of the line profile, which spreads out toward the line wings at the expense of the center; thus, τ_0 decreases, as well as self-absorption. Conversely, a drop of the plasma temperature brings to lower electron density, and self-absorption decreases.
2) A growth of the population density of the lower energy level of transitions implies a higher probability of a photon to be reabsorbed within the plasma; therefore, self-absorption increases, and vice versa.

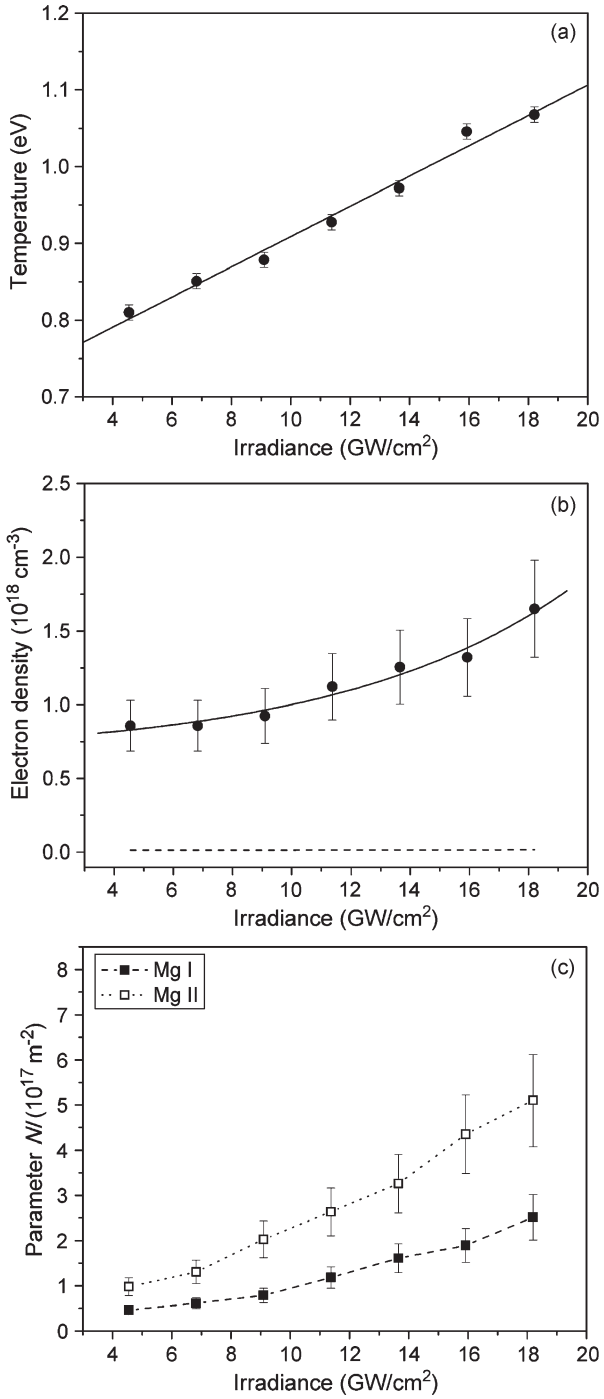

Fig. 11. (a) Temperature, (b) electron density, and (c) Nl parameters of Mg I–II lines for different laser irradiances. Delay: 7 μs, gate: 1 μs. The dashed line indicates the minimum electron number density for the plasma to be in LTE at different laser irradiance. The error in the calculus of the electron density was of 5%–10%. The estimated relative errors in Nl parameters are on the order of 20%.

3) Assuming that the total density of emitters is constant (in our case, $N_{\mathrm{tot}} = N_{\mathrm{Mg\ I}} + N_{\mathrm{Mg\ II}}$), self-absorption is affected by the growth of the plasma volume. As mentioned by Bredice *et al.* in [6], it increases due to the increment of the optical path and decreases due to the diminution of the species density, resulting in a net reduction of self-absorption.

We applied the aforementioned considerations to the results reported in Figs. 4 and 5 in order to interpret the experimentally found self-absorption features of Mg I–II lines. As the plasma evolves with time, the temperature and electron density decrease due to the processes of expansion, cooling, and recombination [Fig. 8(a) and (b)], leading to a drop of emission intensities and to lower Stark broadenings of the lines (Figs. 6 and 7). During the early times of plasma evolution, the behavior of the SA coefficients is difficult to interpret due to the joint action of all the mechanisms aforementioned. Nevertheless, the larger values of the parameters Nl obtained at delay times < 3 μs [Fig. 8(c)] seem to indicate that the prevailing process is the fast expansion of the plume, which is more evident for Mg I because of a larger expansion of the peripheral region, populated mainly by neutrals. In those conditions, self-absorption of both resonance atomic and ionic Mg lines decreased. Moreover, the high electronic density existing in the nucleus at initial times in LIPs causes a further reduction of self-absorption of the Mg II lines 279.55 and 280.27 nm with respect to the Mg I line 285.21 nm. At longer times, the plasma expansion slows down, being $Nl \approx$ const, and the effects of the population of the lower energy levels of the transitions are dominant.

In Fig. 12, we show the coefficients κ_e of Mg I–II lines as a function of the temperature of the plasma, which varies from about 1.8 to 0.8 eV. It can be seen that for the resonance lines, the populations of the lower energy levels grow as the temperature decreases, being more appreciable for the Mg I line 285.21 nm. In this way, self-absorption of those lines grows with time [Fig. 4(a)], as generally expected for transitions involving the fundamental state. The populations of the lower energy levels of the nonresonance lines are considerably lower. The populations of the Mg II lines 279.08 and 279.80 nm decrease as the temperature declines, originating a low self-absorption [Fig. 4(b)]. On the other hand, the Mg I lines 278.14 and 278.30 nm exhibit a distinctive behavior where self-absorption is low at early times. Then, it grows slightly to reach a maximum of about 50% at a delay of about 3 μs, and finally, it decreases again [Fig. 4(b)]. Comparing Figs. 4(b) and 8(a), the maximum self-absorption occurs for a plasma temperature of about 1 eV, which agrees with the value predicted from $\kappa_e(T)$ in Fig. 12(b).

When the pulse energy of the laser is increased maintaining the focusing distance, the irradiance over the sample surface grows and originates a plume with a larger size. At the time of analysis (7 μs), the initial expansion of the plasma is finished, and an increment of the temperature takes place, proportionally to the laser irradiance, accompanied with a moderate growth of the electron density [Fig. 11(a) and (b)]. In consequence, a higher emission intensity of both Mg I and Mg II lines is observed (Fig. 9), together with an exponential increment of the Stark widths of the resonance lines, while those of the nonresonance lines remain approximately constant (Fig. 10). Moreover, an increasing trend of the Nl parameters, with $Nl_{\mathrm{Mg\ II}} > Nl_{\mathrm{Mg\ I}}$, is observed due to a high density of Mg emitters present in the plasma that can be attributed to an increased ablation rate of the target [Fig. 11(c)]. It is known that when the laser irradiance over the sample surface exceeds a certain value, the plasma starts to act like a shield, and its intensity of emission decreases significantly [7], [8]. The threshold irradiance for the shielding effect was estimated to be ≈ 20 GW/cm^2 based on the observation of the plasma shape which, in that case, exhibited a small central core elongated in the direction of laser incidence with a ring around it near the sample surface [17]. In our experiment, the laser irradiance (4.5–18 GW/cm^2) was close to that limit but never surpassed it to make the shielding effect appreciable.

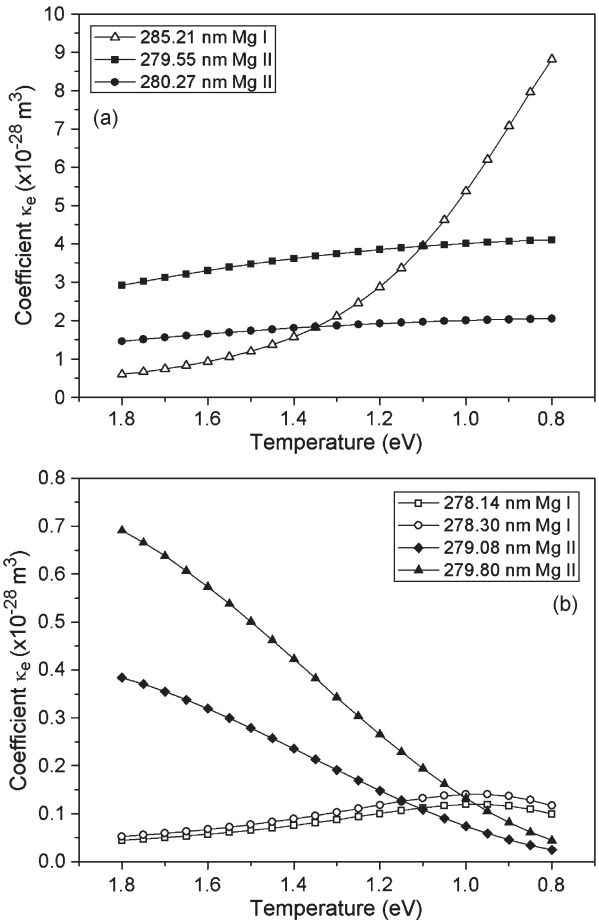

Fig. 12. Coefficients $\kappa_e(T)$ of (3) calculated for the temperatures of the plasma obtained at different delay times. (a) Resonance and (b) nonresonance Mg I–II lines.

In Fig. 13, we show the dependence with the temperature of the calculated values of κ_e of the Mg lines considered in the range of 0.8–1.1 eV, which corresponds to the increase of the laser irradiance. It is observed that the population of the lower energy level of the Mg I resonance line is larger than those of Mg II resonance lines, except for the highest temperatures, and it declines as the plasma temperature grows. In turn, the population of the lower energy levels of Mg II resonance lines is constant, being for the line 279.55 nm twice that of the Mg II line 280.27 nm [Fig. 13(a)]. On the other hand, the population of the nonresonance lines rises with the laser irradiance and the temperature, mainly for Mg II [Fig. 13(b)]. In those conditions, self-absorption of resonance and nonresonance lines of Mg I–II increases due to the higher densities of species in the plasma for the higher irradiance and plasma temperature (Fig. 5). In the case of resonance lines, a plateau is reached for energy values greater than 125 mJ, where the Mg I line 285.21 nm is

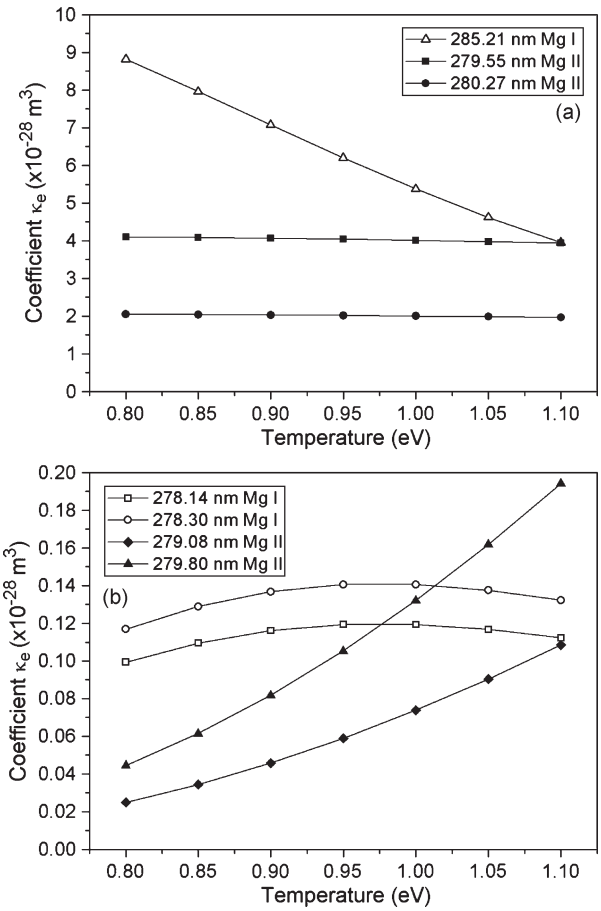

Fig. 13. Coefficients $\kappa_e(T)$ of (3) calculated for the temperatures of the plasma obtained for different laser irradiances. (a) Resonance and (b) nonresonance Mg I–II lines.

less self-absorbed than the Mg II lines. Additionally, the Mg II line 279.55 nm becomes more self-absorbed than the Mg II line 280.27 nm. This result can be explained by the slight growth of the electron density with the irradiance [Fig. 11(b)], which tends to decrease the self-absorption of the lines, mainly for the Mg I line 285.21 nm, which is more sensitive to the Stark broadening since it has a larger electron-impact coefficient.

For the analysis of the line profiles, the gradient effects of temperature and species densities on the line profiles were neglected. Nevertheless, the plasma has some degree of inhomogeneity. The plasma parameters and the optical thicknesses calculated are, in fact, apparent values corresponding to population averaged local values [23]. Nevertheless, a two-region picture of the LIP was considered at the initial times of plasma evolution in order to describe the results obtained because during this stage of plasma dynamics, a fast expansion of the plume takes place, and significant gradients exist in the spatial distributions of the plasma parameters. In this case, the inhomogeneity has an important effect in the line profiles of the more intense spectral lines.

VI. Conclusion

In this paper, we have studied the self-absorption of Mg I–II lines measured at different delay times after the laser pulse from plasmas generated with different laser irradiances on samples with a calcium hydroxide matrix. To this aim, we have simulated the emission spectra in the framework of a homogeneous plasma in LTE and matched them to the experimental line profiles. The fitting procedure does not require a previous estimation of plasma parameters or construction of curves of growth, so it could be easily implemented. Self-absorption of the different lines was evaluated and compensated by calculating their optical thicknesses. Thus, a more reliable determination of the temperature, the electron density, and the Nl parameters was carried out from the optically thin lines retrieved. Then, the self-absorption coefficients calculated were correlated with the different trends of the thermodynamic parameters of the plasma. In fact, we deduced that the variation of self-absorption of spectral lines emitted by a LIP depends, through the optical thickness, on the joint effects of the plasma temperature, the density of species, and the plasma length along the line of sight.

We focused the laser at an optimum distance below the sample surface for which the irradiance over the sample surface is close to the threshold for the shielding effect, but it never surpassed it. On those conditions, the plasmas emitted intense lines and had a spherical shape where the spatial inhomogeneity was minimized. We considered two different stages related to plasma dynamics to interpret the results obtained. At the early times of plasma evolution (delay times shorter than 4 μs), we observed step variations of the temperature, the electron density, and the Nl parameters, suggesting that larger gradients exist in the spatial distributions of the plasma parameters due to the fast expansion of the plume. Thus, we considered a two-region picture of the LIP where a larger expansion of the peripheral region with respect to the core occurs. During the phase of expansion of the plasma, the emission intensity declines abruptly, as well as the temperature and the electron density. The trends of self-absorption for the different lines are difficult to interpret at this stage. At the later times of plasma evolution when it has suffered most of its expansion and cooling, we observed lower gradients of the thermodynamic parameters, from which we inferred that the external region does not have a significant contribution to the total emission. In this case, we considered the results as representative of a "near-uniform" plasma. The emission intensity and the plasma parameters remained approximately constant. We observed that an increment of the laser irradiance originates plasmas with larger sizes. Moreover, a rise of the emission intensity occurs as a consequence of a higher temperature and a larger density of atoms and ions, but only a slight increment of the electron density is produced. At this stage of the plasma evolution, the prevailing mechanism of self-absorption is the variation of population of the lower energy levels of the transitions. Hence, the features of the different lines can be predicted by calculating the $\kappa_e(T)$ coefficients for a suitable range of temperatures (e.g., 0.5–2 eV).

The values obtained for the plasma parameters and the optical thicknesses are apparent values corresponding to population averaged local values. A more realistic model of the LIP would be useful to investigate in detail the distribution of the plasma parameters, mainly during the initial expansion of the plume.

Nevertheless, a good understanding of some of the physical underlying mechanisms was achieved by studying the self-absorption features of spectral lines measured at different experimental conditions. It was shown that the optical thicknesses of emission spectral lines save valuable spectroscopic information that can be used in the diagnostic methods commonly employed in LIBS experiments.

REFERENCES

[1] J. D. Winefordner, I. B. Gornushkin, T. Correll, E. Gibb, B. W. Smith, and N. Omenetto, "Comparing several atomic spectrometric methods to the super stars: Special emphasis on laser induced breakdown spectrometry, LIBS, a future super star," *J. Anal. At. Spectrom.*, vol. 19, no. 9, pp. 1061–1083, 2004.

[2] E. Tognoni, V. Palleschi, M. Corsi, G. Cristoforetti, N. Omenetto, I. Gorhushkin, B. W. Smith, and J. D. Winefordner, "From sample to signal in laser-induced breakdown spectroscopy: A complex route to quantitative analysis," in *Laser-Induced Breakdown Spectroscopy (LIBS) Fundamentals and Applications*, A. W. Miziolek, V. Palleschi, and I. Schechter, Eds., 1st ed. Cambridge, U.K.: Cambridge Univ. Press, 2006, ch. 3.

[3] C. Aragón, J. Bengoechea, and J. A. Aguilera, "Influence of the optical depth on spectral line emission from laser-induced plasmas," *Spectrochim. Acta B, At. Spectrosc.*, vol. 56, no. 6, pp. 619–628, Jun. 2001.

[4] D. Bulajic, M. Corsi, G. Cristoforetti, S. Legnaioli, V. Palleschi, A. Salvetti, and E. Tognoni, "A procedure for correcting self-absorption in calibration free-laser induced breakdown spectroscopy," *Spectrochim. Acta B, At. Spectrosc.*, vol. 57, no. 2, pp. 339–353, 2002.

[5] A. M. El Sherbini, T. M. El Sherbini, H. Hegazy, G. Cristoforetti, S. Legnaioli, V. Palleschi, L. Pardini, A. Salvetti, and E. Tognoni, "Evaluation of self-absorption coefficients of aluminum emission lines in laser-induced breakdown spectroscopy measurements," *Spectrochim. Acta B, At. Spectrosc.*, vol. 60, no. 12, pp. 1573–1579, 2005.

[6] F. Bredice, F. O. Borges, H. Sobral, M. Villagran-Muniz, H. O. Di Rocco, G. Cristoforetti, S. Legnaioli, V. Palleschi, L. Pardini, A. Salvetti, and E. Tognoni, "Evaluation of self-absorption of manganese emission lines in laser induced breakdown spectroscopy measurements," *Spectrochim. Acta B, At. Spectrosc.*, vol. 61, no. 12, pp. 1294–1303, Dec. 2006.

[7] J. A. Aguilera and C. Aragón, "Characterization of laser-induced plasmas by emission spectroscopy with curve-of-growth measurements. Part I: Temporal evolution of plasma parameters and self-absorption," *Spectrochim. Acta B, At. Spectrosc.*, vol. 63, no. 7, pp. 784–792, Jul. 2008.

[8] J. A. Aguilera and C. Aragón, "Characterization of laser-induced plasmas by emission spectroscopy with curve-of-growth measurements. Part II: Effect of the focusing distance and the pulse energy," *Spectrochim. Acta B, At. Spectrosc.*, vol. 63, no. 7, pp. 793–799, Jul. 2008.

[9] H.-Y. Moon, K. K. Herrera, N. Omenetto, B. W. Smith, and J. D. Winefordner, "On the usefulness of a duplicating mirror to evaluate self-absorption effects in laser induced breakdown spectroscopy," *Spectrochim. Acta B, At. Spectrosc.*, vol. 64, no. 7, pp. 702–713, Jul. 2009.

[10] L. Sun and H. Yu, "Correction of self-absorption effect in calibration-free laser-induced breakdown spectroscopy by an internal reference method," *Talanta*, vol. 79, no. 2, pp. 388–395, Jul. 2009.

[11] F. Bredice, O. H. Di Rocco, H. M. Sobral, M. Villagrán-Muniz, and V. Palleschi, "A new method for determination of self absorption coefficients of emission lines in laser-induced breakdown spectroscopy experiments," *Appl. Spectrosc.*, vol. 64, no. 3, pp. 320–323, Mar. 2010.

[12] C. Aragón and J. A. Aguilera, "Characterization of laser induced plasmas by optical emission spectroscopy: A review of experiments and methods," *Spectrochim. Acta B, At. Spectrosc.*, vol. 63, no. 9, pp. 893–916, Sep. 2008.

[13] E. Tognoni, G. Cristoforetti, S. Legnaioli, and V. Palleschi, "Calibration-free laser-induced breakdown spectroscopy: State of the art," *Spectrochim. Acta B, At. Spectrosc.*, vol. 65, no. 1, pp. 1–14, Jan. 2010.

[14] H. Zwicker, "Evaluation of plasma parameters," in *Plasma Diagnostics*, W. Loghte-Holtgreven, Ed. Amsterdam, The Netherlands: North-Holland Publ., 1968, ch. 3.

[15] D. M. Díaz Pace, C. A. D'Angelo, and G. Bertuccelli, "Semiempirical model for analysis of inhomogeneous optically thick laser-induced plasmas," *Spectrochim. Acta B, At. Spectrosc.*, vol. 64, no. 10, pp. 999–1008, Oct. 2009.

[16] J. A. Aguilera, J. Bengoechea, and C. Aragón, "Spatial characterization of laser induced plasmas obtained in air and argon with different laser focusing distances," *Spectrochim. Acta B, At. Spectrosc.*, vol. 59, no. 4, pp. 461–469, Apr. 2004.

[17] D. M. Díaz Pace, C. A. D'Angelo, and G. Bertuccelli, "Calculation of optical thicknesses of magnesium emission spectral lines for diagnostics of laser-induced plasmas," *Appl. Spectrosc.*, vol. 65, no. 10, pp. 1202–1212, Oct. 2011.

[18] H. R. Griem, *Plasma Spectroscopy*. New York: McGraw-Hill, 1964.

[19] H. R. Griem, *Spectral Line Broadening by Plasmas*. New York: Academic, 1974.

[20] NIST Electronic Database. [Online]. Available: http://physics.nist.gov/PhysRefData

[21] I. B. Gornushkin and U. Pannev, "Radiative models of laser-induced plasma and pump-probe diagnostics relevant to laser-induced breakdown spectroscopy," *Spectrochim. Acta B, At. Spectrosc.*, vol. 65, no. 5, pp. 345–359, May 2010.

[22] J. Ritcher, "Radiation of hot gases," in *Plasma Diagnostics*, W. Lotche-Holtgreven, Ed. Amsterdam, The Netherlands: North-Holland Publ., 1968, pp. 9–20.

[23] J. A. Aguilera, J. Bengoechea, and C. Aragón, "Curves of growth of spectral lines emitted by a laser-induced plasma: Influence of the temporal evolution and spatial inhomogeneity of the plasma," *Spectrochim. Acta B, At. Spectrosc.*, vol. 58, no. 2, pp. 221–237, 2003.

Diego M. Díaz Pace, photograph and biography not available at the time of publication.

Cristian A. D'Angelo, photograph and biography not available at the time of publication.

Graciela Bertuccelli, photograph and biography not available at the time of publication.